GFZ
Helmholtz-Zentrum
POTSDAM

Originally published as:

Kim, H., Clauer, C. R., Gerrard, A. J., Engebretson, M. J., Hartinger, M. D., Lessard, M. R., Matzka, J., Sibeck, D. G., Singer, H. J., Stolle, C., Weimer, D. R., Xu, Z. (2017): Conjugate Observations of Electromagnetic Ion Cyclotron (EMIC) Waves Associated with Traveling Convection Vortex (TCV) Events. - *Journal of Geophysical Research*, *122*, 7, pp. 7336—7352.

DOI: http://doi.org/10.1002/2017JA024108

AGU PUBLICATIONS

JGR

Journal of Geophysical Research: Space Physics

RESEARCH ARTICLE

10.1002/2017JA024108

Key Points:
- EMIC waves were observed by interhemispheric magnetometer arrays in association with transient solar wind pressure changes and TCVs
- The waves are well correlated with fluctuating motion of the magnetopause, suggesting compression-associated wave generation
- The multipoint observations show wave events over an extensive latitudinal (L = 6–10) and longitudinal (6 h in MLT) range

Correspondence to:
H. Kim,
hmkim@njit.edu

Citation:
Kim, H., et al. (2017), Conjugate observations of electromagnetic ion cyclotron waves associated with traveling convection vortex events, *J. Geophys. Res. Space Physics*, *122*, 7336–7352, doi:10.1002/2017JA024108.

Received 1 MAR 2017
Accepted 23 MAY 2017
Accepted article online 30 MAY 2017
Published online 17 JUL 2017

©2017. American Geophysical Union. All Rights Reserved.

Conjugate observations of electromagnetic ion cyclotron waves associated with traveling convection vortex events

Hyomin Kim[1], C. Robert Clauer[2], Andrew J. Gerrard[1], Mark J. Engebretson[3], Michael D. Hartinger[2], Marc R. Lessard[4], Jürgen Matzka[5], David G. Sibeck[6], Howard J. Singer[7], Claudia Stolle[5], Daniel R. Weimer[2], and Zhonghua Xu[2]

[1]Center for Solar-Terrestrial Research, New Jersey Institute of Technology, Newark, New Jersey, USA, [2]Center for Space Science and Engineering Research and Department of Electrical and Computer Engineering, Virginia Polytechnic Institute and State University, Blacksburg, Virginia, USA, [3]Department of Physics, Augsburg College, Minneapolis, Minnesota, USA, [4]Space Science Center, University of New Hampshire, Durham, New Hampshire, USA, [5]GFZ German Research Centre for Geosciences, Potsdam, Germany, [6]NASA Goddard Space Flight Center, Greenbelt, Maryland, USA, [7]Space Weather Prediction Center, NOAA, Boulder, Colorado, USA

Abstract We report on simultaneous observations of electromagnetic ion cyclotron (EMIC) waves associated with traveling convection vortex (TCV) events caused by transient solar wind dynamic pressure (P_d) impulse events. The Time History of Events and Macroscale Interactions during Substorms (THEMIS) spacecraft located near the magnetopause observed radial fluctuations of the magnetopause, and the GOES spacecraft measured sudden compressions of the magnetosphere in response to sudden increases in P_d. During the transient events, EMIC waves were observed by interhemispheric conjugate ground-based magnetometer arrays as well as the GOES spacecraft. The spectral structures of the waves appear to be well correlated with the fluctuating motion of the magnetopause, showing compression-associated wave generation. In addition, the wave features are remarkably similar in conjugate hemispheres in terms of bandwidth, quasiperiodic wave power modulation, and polarization. Proton precipitation was also observed by the DMSP spacecraft during the wave events, from which the wave source region is estimated to be 72°–74° in magnetic latitude, consistent with the TCV center. The confluence of space-borne and ground instruments including the interhemispheric, high-latitude, fluxgate/induction coil magnetometer array allows us to constrain the EMIC source region while also confirming the relationship between EMIC waves and the TCV current system.

1. Introduction

Transient phenomena associated with the interaction between the solar wind and magnetosphere such as sudden changes in solar wind parameters (e.g., magnetic fields and flow pressure) have a significant influence on the wave and particle dynamics in the magnetosphere and ionosphere. One of the well-known ground signatures associated with such transient events is magnetic impulse events (MIE) at high latitudes. They are seen as bipolar deflections (positive to negative or vice versa) mainly in the horizontal components of magnetic field data with frequencies approximately in the Pc5 frequency range (f =~ 2–7 mHz or period (t_p) = a few to tens of minutes) for up to half an hour.

MIEs with a traveling structure are often identified as "traveling convection vortices (TCVs)" which are characterized by the vertical pattern of ionospheric convection propagating longitudinally from the dayside to nightside. The vortical ionospheric convection pattern during TCVs is caused by the effect of circular Hall currents produced by a pair of oppositely directed field-aligned currents (FACs) [*McHenry and Clauer*, 1987; *Friis-Christensen et al.*, 1988; *Glassmeier et al.*, 1989; *Kivelson and Southwood*, 1991; *Sibeck et al.*, 2003]. Their longitudinal traveling signatures are due to azimuthal plasma flows when the magnetosphere is buffeted by the transient phenomena. Transient deflections are in the range of several hundreds of nanotesla with maximum occurrences at ~73–75° magnetic latitudes (MLAT) [*Friis-Christensen et al.*, 1988; *Glassmeier et al.*, 1989; *Glassmeier and Heppner*, 1992; *Zesta et al.*, 1999; *Amm et al.*, 2002; *Murr et al.*, 2002; *Zesta et al.*, 2002; *Fillingim et al.*, 2011; *Kim et al.*, 2015]. The location of maximum deflection corresponds to the center of the vortices.

A number of studies [e.g., *Friis-Christensen et al.*, 1988; *Kivelson and Southwood*, 1991; *Sitar et al.*, 1998; *Glassmeier and Heppner*, 1992; *Sibeck et al.*, 1989; *Zesta et al.*, 1999; *Sibeck et al.*, 2003; *Kim et al.*, 2015] suggested buffeting of the magnetosphere due to solar wind dynamic pressure ($P_d = n_p \times v_{sw}^2$ where n_p is proton mass density and v_{sw} is solar wind velocity) perturbations as one of the major generation mechanisms for TCVs. Interhemispheric conjugate behavior of MIE/TCV events has also been reported [e.g., *Kataoka et al.*, 2001; *Murr et al.*, 2002; *Kim et al.*, 2013, 2015], finding that there are interhemispheric asymmetries in some signatures such as convection patterns, spatial scale, and event arrival time.

It is widely accepted that ultralow frequency (ULF) waves in the higher frequency range (0.1–5 Hz) are typically identified as electromagnetic ion cyclotron (EMIC) waves excited by increased temperature anisotropies ($T_\perp > T_\parallel$) of medium energy (~1–100 keV) plasma sheet and ring current ions in the equatorial region of the magnetosphere during geomagnetic storms and substorms [*Anderson et al.*, 1996; *Kozyra et al.*, 1997; *Jordanova et al.*, 2001; *Thorne et al.*, 2006]. Recent studies have shown that a significant number of EMIC wave events also occur during quiet times and/or storm recovery phases [*Usanova et al.*, 2008; *Halford et al.*, 2010, 2015; *Clausen et al.*, 2011; *Kim et al.*, 2016; *Saikin et al.*, 2016]. The wave events are categorized as Pc1 (0.2–5 Hz) and Pc2 (0.1–0.2 Hz) pulsations on the ground. EMIC waves play an important role in causing rapid particle energization and pitch angle scattering into the loss cone and thus electron precipitation loss from the radiation belts into the ionosphere [e.g., *Thorne and Kennel*, 1971; *Lyons and Thorne*, 1972; *Kozyra et al.*, 1997; *Summers and Thorne*, 2003; *Summers et al.*, 2007a, 2007b; *Jordanova et al.*, 2012; *Shprits et al.*, 2016].

It has also been reported that compression of the magnetosphere due to transient phenomena can cause EMIC waves [e.g., *Anderson et al.*, 1992; *Anderson and Hamilton*, 1993; *Engebretson et al.*, 2002; *Usanova et al.*, 2010, 2012; *Cho et al.*, 2016; *Park et al.*, 2016; *Saikin et al.*, 2016]. TCV events, which are closely associated with compression and decompression of the magnetosphere due to sudden P_d change, also contribute to generation of EMIC waves [e.g., *Arnoldy et al.*, 1988, 1996; *Engebretson et al.*, 2013; *Posch et al.*, 2013].

This paper presents simultaneous observations of TCVs and EMIC waves in association with transient P_d changes in the magnetosphere. Our companion paper by *Kim et al.* [2015] reported details of the TCV events. In this paper, we report on EMIC waves closely correlated with the TCV events using data from interhemispheric conjugate ground-based magnetometer arrays in Greenland, Canada, and Antarctica as well as various spacecraft near the magnetopause and at geosynchronous orbit. The extensive conjugate ground network in both hemispheres along with well-situated satellites made it possible to perform a thorough, systematic investigation of wave generation and propagation and to relate these waves to solar wind-magnetosphere coupling processes.

2. Data Set

For observations of solar wind plasma parameters, we used high time resolution (1 min) OMNI data [*King and Papitashvili*, 2005] processed from magnetic field and plasma measurements recorded by the Advanced Composition Explorer (ACE) and Wind spacecraft and time shifted to the nose of the Earth's bow shock. ACE 16 s Magnetic field (MFI) and 64 s Solar Wind Electron Proton Alpha Monitor (SWEPAM) data are also presented.

Magnetic field and particle data from the Time History of Events and Macroscale Interactions during Substorms (THEMIS) spacecraft (A, D, and E) [*Angelopoulos*, 2008] were used to investigate the transient events near the magnetopause. Spin resolution (~3 s) magnetic field data from the fluxgate magnetometers (FGM) [*Auster et al.*, 2008] aboard the spacecraft are used to present magnetic field perturbations near the magnetopause. Three-dimensional ion velocity distributions shown in this paper were calculated based on ion fluxes measured by the electrostatic analyzer (ESA) [*McFadden et al.*, 2008] over the energy range of 5 eV to 25 keV. Among the three operation modes (full, reduced, and burst), this paper presents ESA data obtained in the burst mode which provides 32 energy levels and 88 solid angles. The Space Physics Environment Data Analysis Software (SPEDAS) was used to plot the THEMIS data.

Magnetic field perturbations and wave events in the inner magnetosphere were observed by the magnetometers (512 ms time resolution) aboard the Geostationary Operational Environmental Satellite (GOES) spacecraft (13 and 15).

All the space-borne magnetometer data in this paper are presented in the Geocentric Solar Ecliptic (GSE) coordinate system except for GOES satellite data which are given in the so called "PEN" coordinate system, in which B_P is a magnetic field vector component pointing northward, perpendicular to the orbit plane

Table 1. Geographic and Geomagnetic Locations of the Magnetometer Stations Presented in This Study[a]

Region	Station	Station Code	Geographic		Geomagnetic		MLT MN[b] in UT
			Lat. (deg)	Long. (°E)	Lat. (deg)	Long. (°E)	
Northern Hemisphere	Kangerlussuaq	STF	67.0	309.3	72.1	40.0	2.5
	Iqaluit	IQA	63.8	291.5	71.7	15.2	4.2
Southern Hemisphere	AGO3	AGO3	−82.8	28.6	−72.1	41.0	2.0
	AAL-PIP PG3	PG3	−84.8	37.6	−73.6	36.8	2.4
	South Pole	SPA	−90.0	–	−74.2	19.4	3.6
	AAL-PIP PG2	PG2	−84.4	58.0	−75.3	39.2	2.2
	AGO1	AGO1	−83.9	129.6	−80.3	17.33	3.8
	AGO5	AGO5	−77.2	123.5	−87.0	29.5	2.9
	Halley	HBA	−75.6	333.4	−62.1	29.9	2.7

[a]The geomagnetic coordinates of the stations are obtained from the International Geomagnetic Reference Field (IGRF) Corrected Geomagnetic (CGM) model for Epoch 2013 using the modelweb facility at NASA/Goddard Space Flight Center (http://modelweb.gsfc.nasa.gov/models/cgm/cgm.html).
[b]MLT MN: MLT midnight.

(parallel to Earth's spin axis) and B_E points earthward, being perpendicular to B_P. B_N completes the Cartesian coordinates and points eastward.

The Special Sensor J (SSJ) instrument aboard the Defense Meteorological Satellite Program (DMSP) satellite was used for observations of precipitating electrons and ions at an altitude of ~850 km over a range of energies from 30 eV to 30 keV.

Ground magnetic field data were obtained from fluxgate and induction coil magnetometers located in magnetically conjugate stations in Greenland, Canada, and Antarctica. The fluxgate magnetometer at Kangerlussuaq (STF) is operated by Technical University of Denmark (DTU) and provides 1 s (time stamped for the beginning of the 10 s interval) magnetic field data. The fluxgate magnetometer (1 s resolution) at Iqaluit (IQA), Nunavut, Canada, is operated by Natural Resources Canada (NRCan). The Antarctic stations include Halley Station (HBA), South Pole Station (SPA), three (AGO1, AGO3, and AGO5) Automatic Geophysical Observatories (AGOs) [*Mende et al.*, 2009; *Melville et al.*, 2014], and two (PG2 and PG3) Autonomous Adaptive Low-Power Instrument Platform (AAL-PIP) systems [*Musko et al.*, 2009; *Clauer et al.*, 2014]. The ground stations used in this study are shown in Table 1 and Figure 5 in section 3.2. All of the Antarctic stations provide fluxgate magnetic field data of 1 s resolution. The ground fluxgate magnetometers conform to the "HEZ" coordinate system, in which H is local geomagnetic northward in the horizontal plane, Z is downward toward the earth, and E completes the right-hand rule pointing eastward.

For observations of wave events, also presented are data from ground-based induction coil magnetometers colocated at the stations listed above. The induction coil magnetometers provide two-axis time-varying magnetic field (dB/dt) data in local geomagnetic coordinates with X aligned along the geomagnetic north-south direction and Y the east-west at the rate of 10 samples/s. The induction coil magnetometers are now incorporated into a network called the Magnetic Induction Coil Array (MICA).

3. Observations

The events presented in this paper are based on the solar wind pressure impulse-associated TCV events reported by *Kim et al.* [2015]. During the two consecutive TCV events observed on 19 January 2013, EMIC waves were also measured by a network of induction coil magnetometers in conjugate hemispheres. The impulse events were caused by sudden increases in P_d, which are observed as fluctuations of the magnetopause boundary layer by the THEMIS spacecraft and as a magnetospheric compression by the GOES spacecraft. EMIC waves were also seen by the GOES spacecraft in association with the compression. During the events, only 3 s magnetic field data were provided by the THEMIS spacecraft and thus no observations of EMIC waves, which require higher time resolution data, were available. The interhemispheric ground fluxgate magnetometers clearly detected a series of TCV events in response to the transient phenomena, while the induction coil magnetometer array measured EMIC waves which are well correlated with the TCVs.

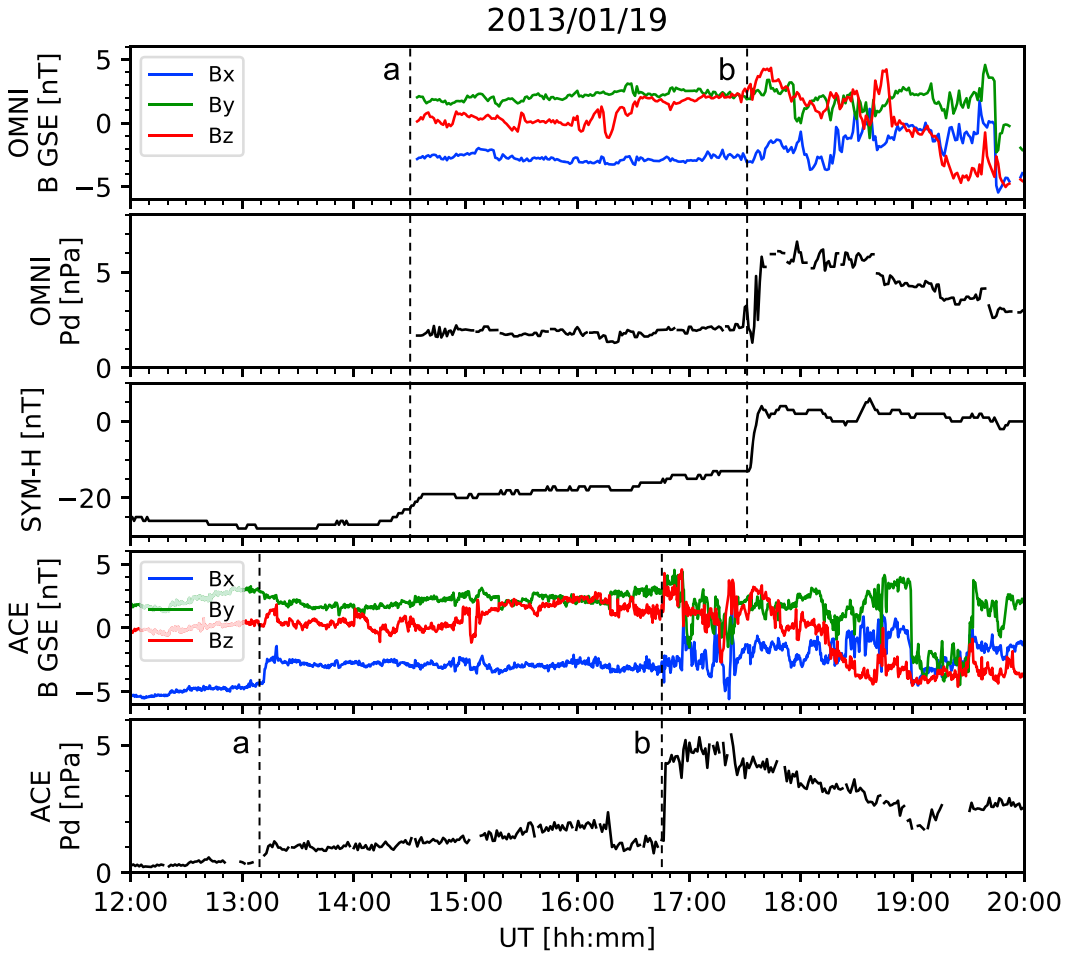

Figure 1. OMNI (time shifted to the bow shock) and ACE data showing the IMF, flow pressure (P_d), and *SYM-H* index for the events on 19 January 2013. The vertical dashed lines (a and b) indicate the onset times of the transient events associated with sudden increases in P_d. Note the time delay between OMNI and ACE data.

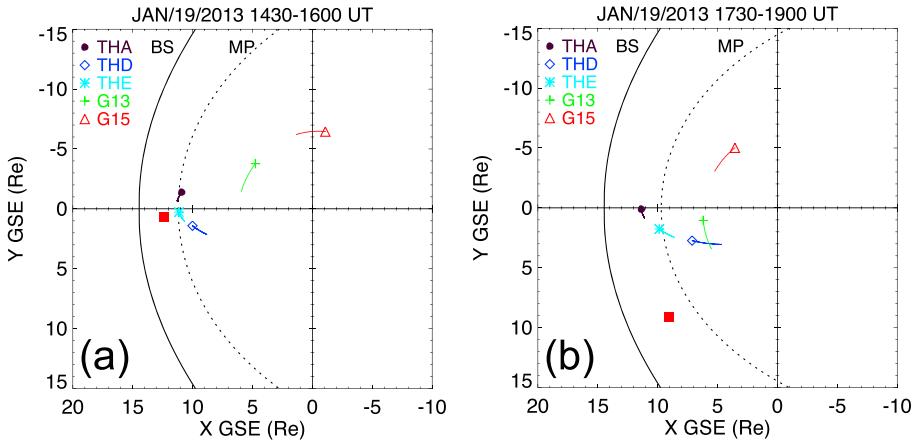

Figure 2. Spacecraft positions during (a) Event 1 and (b) Event 2: THEMIS A (THA), THEMIS D (THD), THEMIS E (THE), GOES 13 (G13), and GOES 15 (G15). The symbols in the orbit plots indicate the initial locations of each spacecraft during the time period shown on top of the panel. The bow shock (BS) and magnetopause (MP) locations are obtained using the models by *Fairfield* [1971] and *Shue et al.* [1997], respectively. The equatorial intersections of the magnetic fields traced back from the TCV centers reported by *Kim et al.* [2015] are marked with red squares.

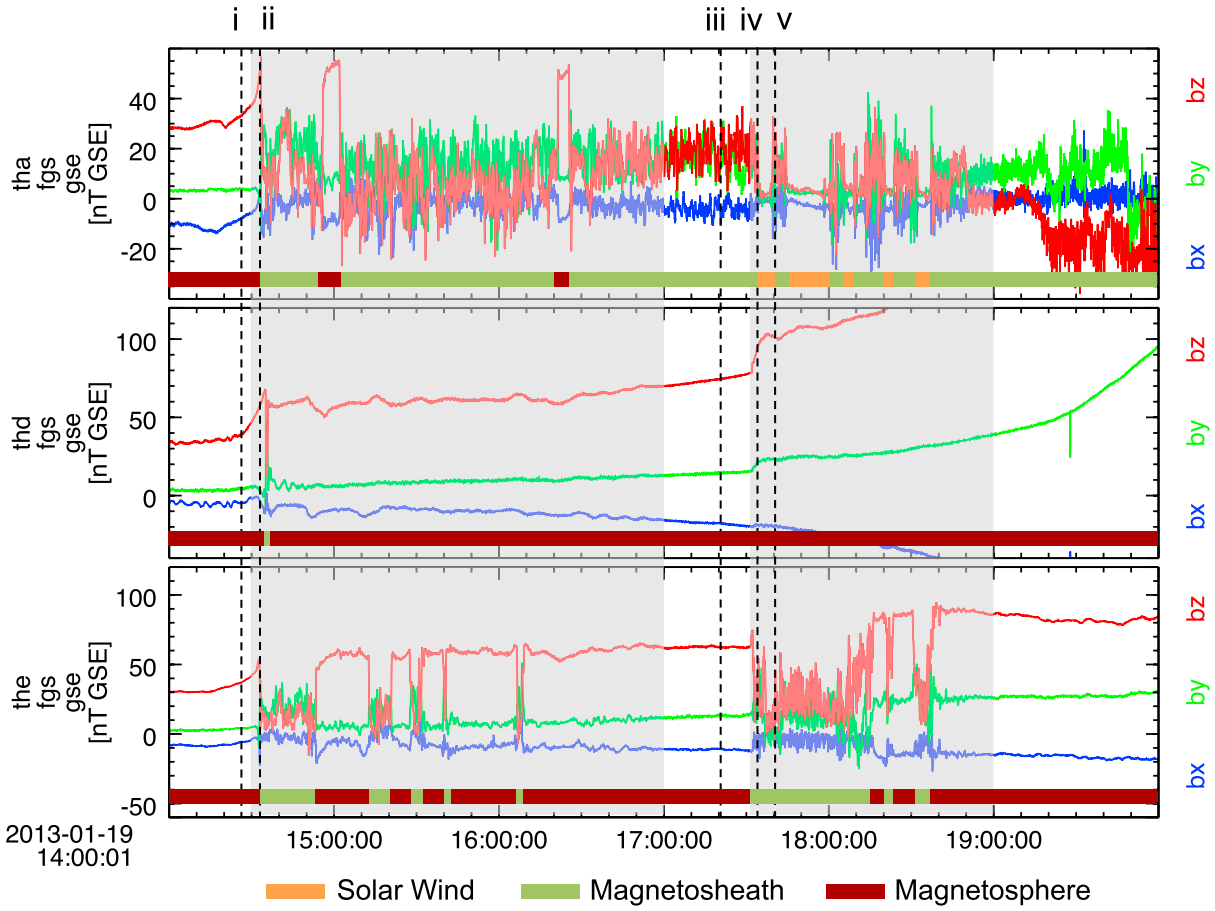

Figure 3. Magnetic field data obtained by (top) THEMIS A, (middle) THEMIS D, and (bottom) THEMIS E during the events presented in this study. The horizontal color bars below each panel denote the regions where each spacecraft was situated. The two grey boxes indicate the time periods of the EMIC wave events which will be described in the following section. The vertical dashed lines are mentioned in section 4.

Although Figures 1 to 3 have already been reported in our companion paper [*Kim et al.*, 2015], here we still show the figures and related observational descriptions to use as supporting materials for the wave events.

3.1. Transient Events in Space

OMNI and ACE data are presented in Figure 1 [cf. *Kim et al.*, 2015, Figure 6a], showing two consecutive transient events observed on 19 January 2013. The first and second events began at 14:30 UT (the vertical dashed line a, "Event 1" hereinafter) and 17:30 UT (the vertical dashed line b, "Event 2" hereinafter), respectively. Note the time delay between OMNI and ACE data. While the OMNI data in this figure contain a data gap (before the vertical line a), a transient event is confirmed in the upstream ACE data where we observe a P_d increase of 1 nPa over about 5 min for Event 1. In addition, the *SYM-H* index (Figure 1, third panel) can be interpreted as evidence for a magnetospheric compression due to the pressure impulse producing a field increase of 8 nT over 20 min [*Kim et al.*, 2015]. A P_d increase of 4.5 nPa over 5 min and the compression of the magnetosphere (18 nT over 8 min) are seen in the flow pressure data and *SYM-H* index during Event 2. The magnetic field data (Figure 1, first panel) indicate that the interplanetary magnetic field (IMF) was predominantly northward or near 0 (ACE data also confirm this) during both events.

Spacecraft positions in the GSE *X-Y* plane during Events 1 and 2 are illustrated in Figure 2 [cf. *Kim et al.*, 2015, Figures 6c and 6f], in which the three THEMIS spacecraft were fortuitously located near the magnetopause. The bow shock locations are obtained using the static model by *Fairfield* [1971]. The magnetopause locations are estimated using the dynamic model by *Shue et al.* [1997], which are based on the IMF and solar wind dynamic pressure values during the events. The equatorial intersections of the magnetic fields traced back from the TCV centers are marked with red squares in this figure. The intersections are estimated by tracing the magnetic field lines of each TCV center to the equatorial plane using a magnetic field tracing tool

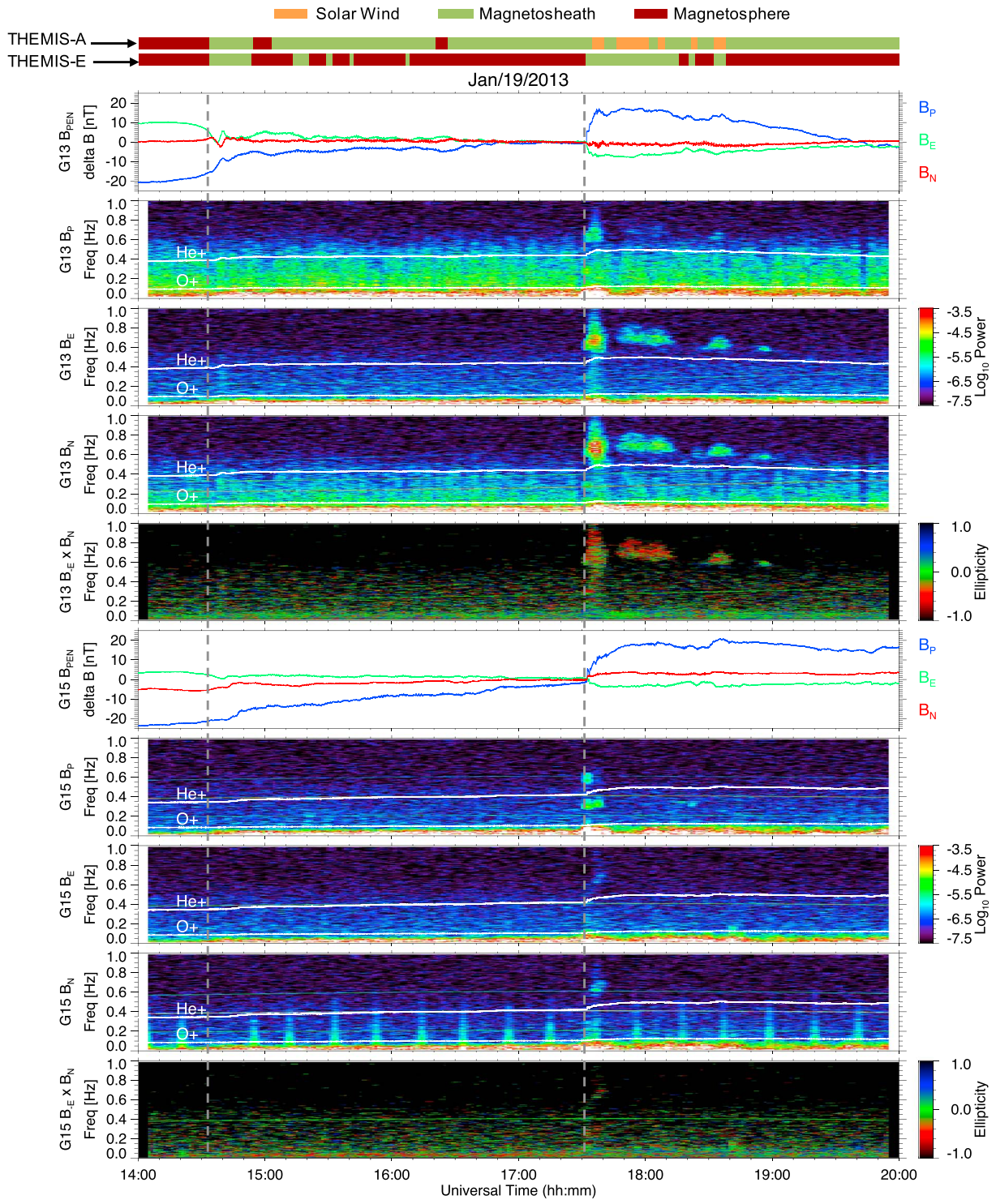

Figure 4. Magnetic field data obtained by the (first to fifth panels) GOES 13 and (sixth to tenth panels) GOES 15 spacecraft during the events presented in this study. The line plots are background-removed magnetic fields (δB) for each component (B_P, B_E, and B_N). The spectrograms display the wave power in each component and polarization (ellipticity) in spectral domains. The white traces in the wave power spectrograms denote local helium and oxygen gyrofrequencies. The vertical dashed lines indicate the onset times of the transient events associated with sudden increases in P_d. The horizontal color bars used in Figure 3 are shown on top of the figure to show the temporal relationship between the magnetopause fluctuations and wave activity.

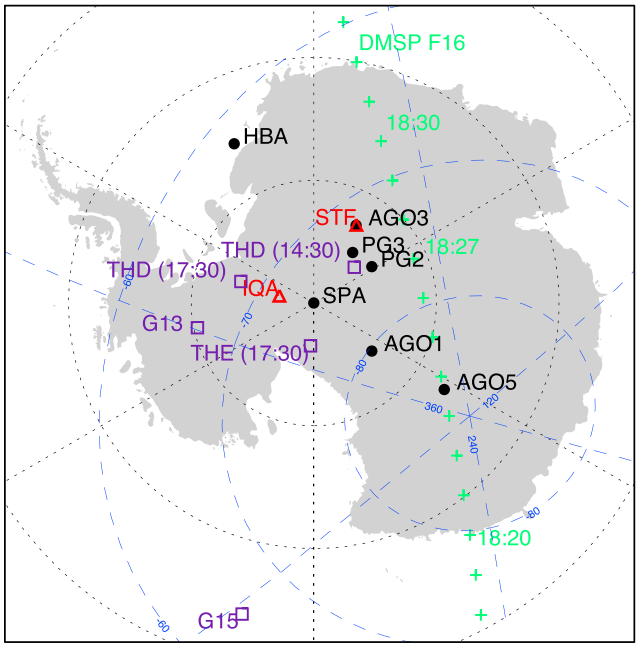

Figure 5. Map of Antarctica showing the locations of the Antarctic stations including Halley Station (HBA), South Pole Station (SPA), three (AGO1, AGO3, and AGO5) of the automatic geophysical observatories (AGO), and Autonomous Adaptive Low-Power Instrument Platform (AAL-PIP) systems (PG2 and PG3), marked by the solid black circles. The red triangles indicate the locations of Iqaluit (IQA) and Kangerlussuaq (STF) magnetometer stations geomagnetically projected into the Antarctic. The magnetic footprints of THEMIS D (THD), THEMIS E (THE), and GOES 13 (G13) spacecraft locations are marked by purple squares with times in parenthesis. The locations of THEMIS A during the two events and THEMIS E during Event 1 are not shown here due to their orbits near the open field lines. The green crosses mark the magnetic footprint of the DMSP F16 spacecraft and its overflight times during Event 2 (described in section 4). The black dotted lines and blue dashed lines represent geographic and (IGRF-based) geomagnetic latitudes and longitudes, respectively.

(Interactive Data Language (IDL) GEOPACK) based on the International Geomagnetic Reference Field (IGRF) and Tsyganenko model (T01) [*Tsyganenko*, 2002a, 2002b].

Magnetic field variations showing radial motion of the magnetopause are observed by THEMIS A, D, and E as presented in Figure 3 [cf. *Kim et al.*, 2015, Figures 6b and 6e]. The three spacecraft, which were positioned inside the magnetosphere before the onset of Event 1, observed the compression of the magnetosphere (~20 nT increase in B_z) at 14:30 UT (~11:30 MLT). After the onset, both spacecraft A and E measured fluctuating motion of the boundary as the satellites move back and forth between the magnetosphere (higher and steady magnetic fields) and magnetosheath (characterized by its "noisy" magnetic fields). Specifically, THEMIS A entered the magnetosheath right after the compression at 14:30 UT and returned to the magnetosphere at 14:52 UT for about 5 min. THEMIS E observed more fluctuating signatures during this event. On the other hand, THEMIS D only briefly moved into the magnetosheath at the peak of the compression. As shown in Figure 2, spacecraft A and E were near the magnetopause while spacecraft D was further inside the magnetosphere during Event 1.

Event 2 starting at 17:30 UT (~12:30 MLT) also shows radial motion of the magnetopause as observed by the three THEMIS spacecraft, which were located in the magnetosheath (THEMIS A), near the magnetopause (THEMIS E), and inside the magnetosphere (THEMIS D) before the onset (see Figure 2). Similar to Event 1, while THEMIS A and E observed the fluctuating boundary, THEMIS D measured an increase in the magnetic fields (B_z component in particular, ~30 nT) inside the magnetosphere. During Event 2, spacecraft A entered the solar wind (weaker and steady magnetic fields) approximately between 17:45 UT and 18:00 UT. Solar wind entries of THEMIS A occurred several times briefly during Event 2. The horizontal color bars in this figure denote the regions where each THEMIS spacecraft was situated.

Figure 4 presents magnetic field data from the GOES 13 and 15 spacecraft. The compression of the magnetosphere associated with the two transient events starting at 14:30 UT and 17:30 UT is clearly seen

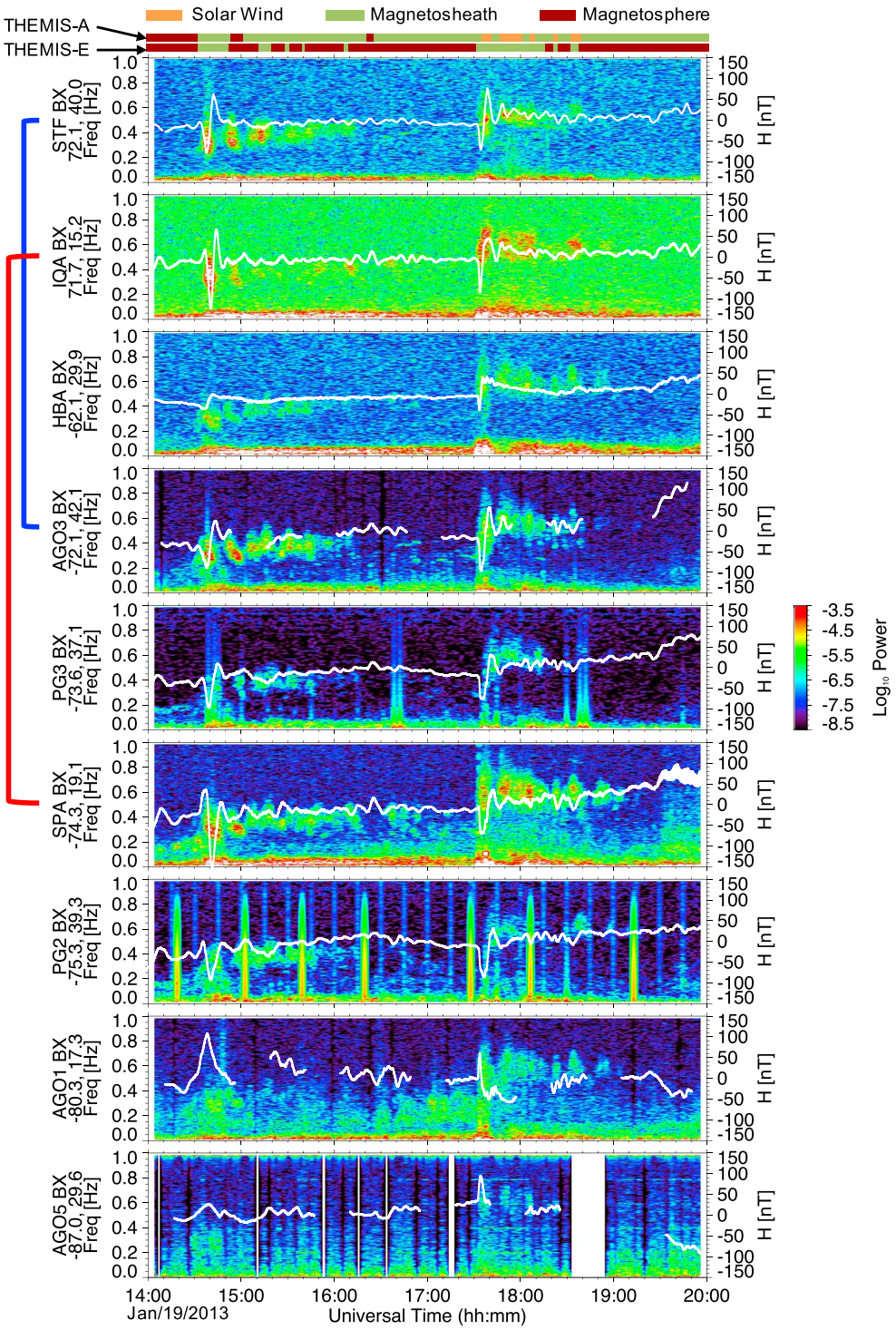

Figure 6. FFT spectrograms of ground-based induction coil magnetometer data (*X* axis) showing ULF Pc1 waves during the transient events. The white traces overplotted with the spectrograms represent fluxgate magnetometer data (H components) obtained at the same stations. The panels are stacked in order of magnetic latitude, the top panel being the highest (northernmost) and the bottom one being the lowest (southernmost). The numbers below each station code are the latitudes and longitudes in CGM coordinates. Blue and red brackets mark the interhemispheric conjugate station pairs: STF-AGO3 and IQA-SPA. The temporal relationship between the magnetopause fluctuations and wave activity is shown by the color bars at the top of the figure (cf. Figures 3 and 4). The quasiperiodic broadband bursts in the PG2 data are due to short missing data gaps, which therefore cause broadband spectral structures when data are Fourier transformed.

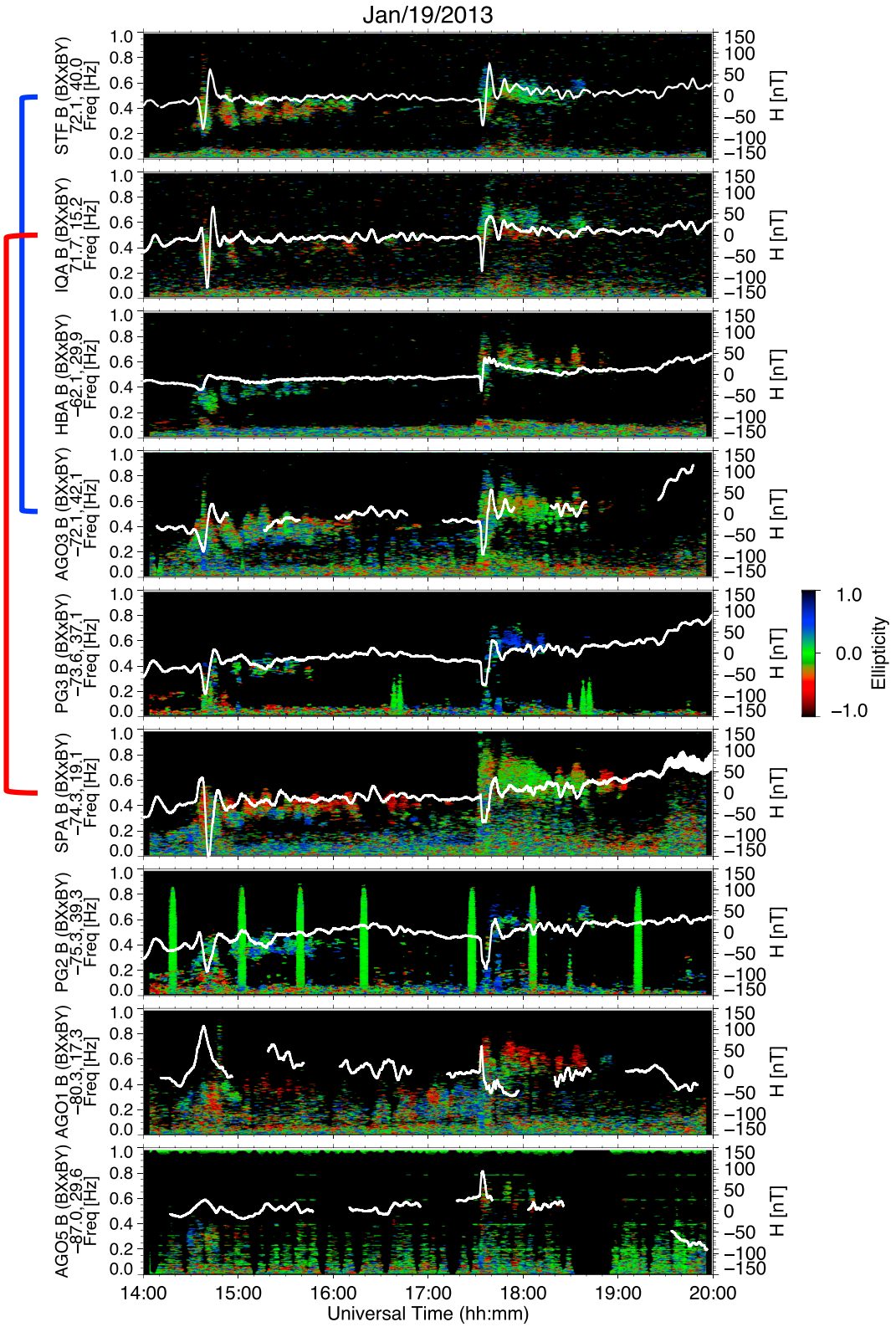

Figure 7. Same as Figure 6 but for polarization (ellipticity) of the induction coil magnetometer data.

by the two GOES spacecraft as shown in the line plots (Figure 4, first and sixth panels). For the line plots, the baseline of each component (mean value of the data) is subtracted from the original GOES satellite data to show magnetic field variations only. No wave activity is seen during Event 1, whereas band-limited wave structures are observed during Event 2. The wave event observed by GOES 13 is both left-hand (red colors) and linearly (green colors) polarized. In this paper, we define left-hand, right-hand, and linear polarization as being ellipticity, $\varepsilon \leq -0.2$, $\varepsilon \geq 0.2$, and $|\varepsilon| < 0.2$, respectively, as also defined in *Anderson et al.* [1992]. GOES 15 data show a very brief occurrence of wave activity during Event 2. It should be noted that the magnetometers aboard the GOES spacecraft provide 512 ms (~1.95 Hz) time resolution data and thus the frequencies of the wave events may be slightly different from actual values because they are close to the Nyquist frequency (0.975 Hz). Placed on top of the figure are the same color bars used in Figure 3 to show the temporal relationship between the magnetopause fluctuations and wave activity.

3.2. Conjugate Observations of EMIC Waves on the Ground

The companion paper by *Kim et al.* [2015] reported interhemispheric conjugate observations of TCV events in association with the transient events presented in the previous section. The TCVs were observed primarily by the ground fluxgate magnetometers in Greenland and Canada and their geomagnetically conjugate stations in Antarctica along the 40° magnetic meridian. Some of the stations are equipped with induction coil magnetometers that detected waves during the TCV events. The ground stations used in this study are shown in Table 1 and Figure 5. As shown in the map, the Antarctic induction coil magnetometers, in particular, are deployed over a large latitudinal extent, making it possible to estimate the wave source region which otherwise is quite challenging due to horizontal wave propagation in the ionospheric waveguide [e.g., *Kim et al.*, 2011]. In addition, the network establishes interhemispheric conjugate pairs, e.g., Kangerlussuaq (STF)-AGO3 and Iqaluit (IQA)-South Pole (SPA), which provide important information about the interhemispheric conjugate behavior of wave propagation from the magnetosphere to the ionosphere.

The induction coil magnetometer array in the conjugate hemispheres detected ULF Pc1 waves which are interpreted as EMIC waves associated with the TCVs as shown in Figure 6. The panels are stacked in order of magnetic latitude, the top panel being the highest (northernmost) and the bottom one being the lowest (southernmost). The fast Fourier Transform (FFT) spectrograms of the induction coil magnetometer data display Pc1 waves during the transient events. The white traces overplotted with the spectrograms represent fluxgate magnetometer data (H components) obtained at the same stations. The fluxgate magnetometer data shown here are baseline-removed (mean value subtraction from the original data) to isolate TCV signatures from the background. The bipolar deflections of the fluxgate (low period) magnetic field data at 14:30 UT (Event 1) and 17:30 UT (Event 2) are one of the typical signatures of TCVs as described in *Kim et al.* [2015]. The local times for the events are 12:30 MLT and 15:30 MLT, respectively. It is clearly seen that the onsets of wave events coincided with the TCVs. The blue and red brackets in the figure mark the two interhemispheric conjugate pairs: STF-AGO3 and IQA-SPA (see Table 1 for their locations). The color bars used in Figure 3 are shown on top of the figure to show the temporal relationship between the magnetopause fluctuations and wave activity. Figure 7 shows polarization (ellipticity) of the wave events shown in Figure 6.

Kim et al. [2015] reported that the maximum disturbances were observed near STF in the Northern Hemisphere and SPA in the Southern Hemisphere among those observed by the stations along the 40° magnetic meridian during both events. The maximum disturbances correspond to each vortex center, to which the FACs produced in association with the TCVs are mapped. As mentioned earlier, the equatorial intersections of the TCV centers are marked with red squares in Figure 2. The wave spectral power also appears to be related to the TCV centers: that is, the activity at STF and SPA display strongest spectral power and clear band-limited and temporal signals well above the background level. The waves observed at STF and SPA during Event 1 are predominantly left-hand polarized, while the waves observed at the same stations during Event 2 are linearly polarized (see Figure 7).

4. Discussion

The literature listed earlier suggests that P_d is a main driver for TCVs. The two events reported in our paper are also closely associated with transient changes in P_d. The solar wind data (Figure 1) show that the increase (rate) of P_d is 1 nPa (0.2 nPa/min) for Event 1 and 4.5 nPa (0.9 nPa/min) for Event 2. Accordingly, the increase (rate) of magnetospheric compression is 8 nT (0.4 nT/min) and 18 nT (2.25 nT/min) based on the *SYM-H* index for the two events, respectively. Both events were observed by the THEMIS spacecraft at similar local times

(near noon). The geomagnetic conditions were quiet during the two events (e.g., $Kp = 1-2$). Interestingly, the P_d change for Event 2 presents a wave-like feature, of which the frequency (~5.5 mHz) appears to be in the ULF Pc5 range. However, such a feature is not clearly seen in the ACE data. Nevertheless, it appears that the periodic structure in P_d has little effect on the TCV and EMIC wave events because the inner magnetospheric signatures observed by the THEMIS D (Figure 3) and GOES (Figure 4) spacecraft and ground magnetometers (Figure 6) show a monotonic compression and its responses (i.e., TCVs and EMIC waves) with no such periodic features observed.

The solar wind changes and magnetospheric compression appear to be related to the spectral features of the wave activity in space (Figure 4) and on the ground (Figure 6). That is, the center (mean) frequency increases with the pressure increase (and thus magnetospheric compression). The center frequency of Event 2 EMIC waves is higher (0.50–0.60 Hz) than that of Event 1 (0.30–0.35 Hz), indicating that the higher frequencies are due to higher background magnetic fields caused by the compression and thus higher local gyrofrequencies. We also note that the spectral features of the wave events are remarkably similar in the conjugate hemispheres in terms of bandwidth, quasiperiodic wave power modulation, and polarization. The companion paper by *Kim et al.* [2015] reported well-defined interhemispheric features of the TCV events.

Some earlier studies have reported that EMIC waves can be modulated by longer-period ULF waves such as Pc3–5 pulsations [e.g., *Rasinkangas and Mursula*, 1998; *Loto'Aniu et al.*, 2009]. In fact, boundary phenomena due to solar wind-magnetosphere interactions (e.g., solar wind dynamic pressure impulses or Kelvin-Helmholtz Instability) can generate long-lasting ULF waves [e.g., *McHenry et al.*, 1990; *Clauer and Ridley*, 1995; *Fujita et al.*, 1996; *Clauer*, 2003; *Hasegawa et al.*, 2004; *Claudepierre et al.*, 2008; *Piersanti et al.*, 2012; *Shi et al.*, 2013; *Hartinger et al.*, 2013, 2015. The EMIC wave events reported in our study, however, do not appear to be associated directly with such ULF waves because of the clear signature of the magnetospheric radial motion and its connection with the wave generation. Instead, we suggest that the wave activity is associated with the abrupt changes of the magnetic fields, thus causing proton temperature anisotropies to increase.

Inward and outward motion of the magnetopause is clearly shown in Figure 3. While THEMIS A was passing along the magnetopause boundary during Event 1, THEMIS E was moving antisunward from the boundary to the magnetosphere. Perhaps, this is why the quasiperiodic disturbances were detected by the spacecraft E between 14:30 UT and 16:10 UT. On the other hand, spacecraft A was in the magnetosheath during most of the first event period (14:30–17:00 UT) and the outward motion was seen only briefly (~14:55–15:00 UT and 16:20–16:25 UT). The fluctuations seen from the THEMIS E magnetic field data (especially the beginning of the fluctuations, ~14:30–15:30 UT) are also observed in the ground-based induction coil magnetometer data (Figure 6). That is, the quasiperiodic fluctuation (approximate period of 20 min) in spectral wave power during Event 1 appears to be correlated with the fluctuating motion of the magnetopause observed by THEMIS E. The first wave activity (14:30–14:40 UT) began with the first compression at 14:30 UT. The second wave activity (14:50–15:00 UT) is associated with the decompression at 14:50 UT. Similarly, the third wave activity (15:10–15:20 UT) coincided with the compression at 15:10 UT. Such a tendency persisted until ~16:30 UT (Event 1). This compression/decompression-associated wave events are also clearly seen during Event 2. Color bars demarcating the three different regions (solar wind, magnetosheath, and magnetosphere) are used in Figures 3, 4, and 6 to help readers compare the events shown in THEMIS, GOES, and ground magnetometer data. Note that higher time resolution THEMIS data (both *B* and *E*), which are necessary for EMIC wave observations, are unavailable for these events.

Solar wind pressure-associated EMIC wave observations at geosynchronous orbit have been reported [e.g., *Kim et al.*, 2016; *Park et al.*, 2016]. The transient magnetospheric compression during the TCVs was also clearly measured by the GOES spacecraft as shown in Figure 4. The change is most dominant in the northward component (B_P) for both events beginning at ~14:30 UT and ~17:30 UT, respectively. In association with the transient events, EMIC waves over ~0.6–0.8 Hz were observed during Event 2, whereas no wave activity was seen during Event 1. Perhaps due to a local time effect, the transient compression is more pronounced in the GOES 13 data than in the GOES 15 data during both events. Likewise, the waves observed by GOES 13 are more structured. During both events, GOES 15 was situated farther away from the transient event seen by THEMIS than GOES 13 in terms of local time (see Figure 2 for spacecraft locations). The spectral power variation in the GOES 13 data during Event 2 is quite similar to that in the ground data. This indicates that the wave power is modulated by the magnetospheric transient fluctuations as also shown in the relationship between the THEMIS and ground magnetometer data.

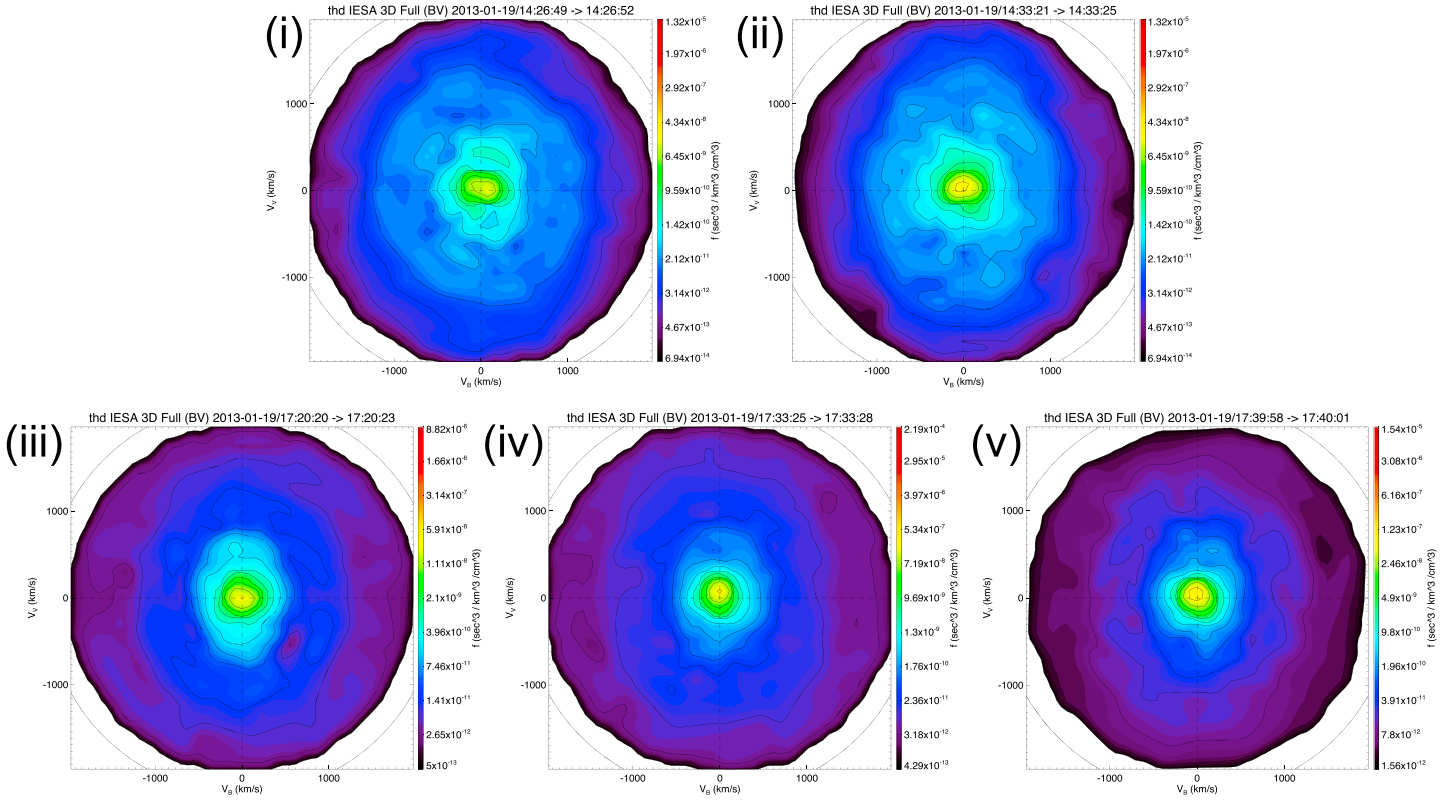

Figure 8. Three-dimensional ion velocity distributions calculated based on ion fluxes measured by the electrostatic analyzer (ESA) aboard the THEMIS D spacecraft for the times shown in Figure 3 (vertical dashed lines (i) to (v)). The *x* and *y* axes of the plots represent parallel and perpendicular components of ion velocities. The flux levels are color coded.

The absence of wave activity in the GOES data during Event 1 (while the ground data show very well-defined waves) might imply that the compression-related EMIC waves were localized both in *L* and local time. The locations of each spacecraft and the ground signature (red squares) in Figure 2 suggest this. On the other hand, during Event 2, the wave activity was observed in both GOES and ground data even though the local time separation is ~3 h (GOES 13) and ~6 h (GOES 15). Again, we note that the pressure increase is moderate for Event 1 and larger for Event 2. This may affect the global extent of EMIC wave generation. The magnetic footprints of the spacecraft are also shown in Figure 5 to help compare the locations of the transient events in space and signatures on the ground. Considering the ground signatures, the longitudinal extent of the wave activity for Event 2 is at least ~6 h in MLT (see the red square and GOES 15 location as shown in Figure 2).

Once waves enter the ionosphere, they propagate horizontally in the ionospheric waveguide (duct) [e.g., *Fraser*, 1975; *Fujita and Tamao*, 1988; *Kim et al.*, 2010, 2011], and therefore the wave source (near the field lines in the ionosphere along which waves propagate from the magnetosphere) can be estimated by comparing wave power and spectral structure. From a visual inspection of the wave events presented in the ground data (Figure 6), the wave sources in magnetic latitude are estimated to be near STF (72.1° MLAT) or IQA (71.7° MLAT) in the Northern Hemisphere and SPA (−74.3° MLAT) in the Southern Hemisphere. We note here that the induction magnetometers are not precisely intercalibrated. Nevertheless, one can still use the data to estimate an approximate wave source location by assessing the definition of spectral structures. Wave polarization patterns can also be used to locate the wave source because EMIC waves are typically left-hand polarized near the source field line on the ground [e.g., *Kim et al.*, 2011, and references therein]. The wave event at SPA during Event 1 was predominantly left-hand polarized. The second event, however, did not show left-hand polarization at the aforementioned stations. It is not clear what prevented left-hand waves from reaching the ground during Event 2. Strong waves were not observed at AGO5, which is located above the auroral zone in the polar cap. This region is typically thought to be located under open field lines mapping to the lobes of the tail and often directly connected to solar wind field lines. The lack of wave signatures could be because AGO5 is located far away from the wave source or its location in the region of open field lines is more susceptible to

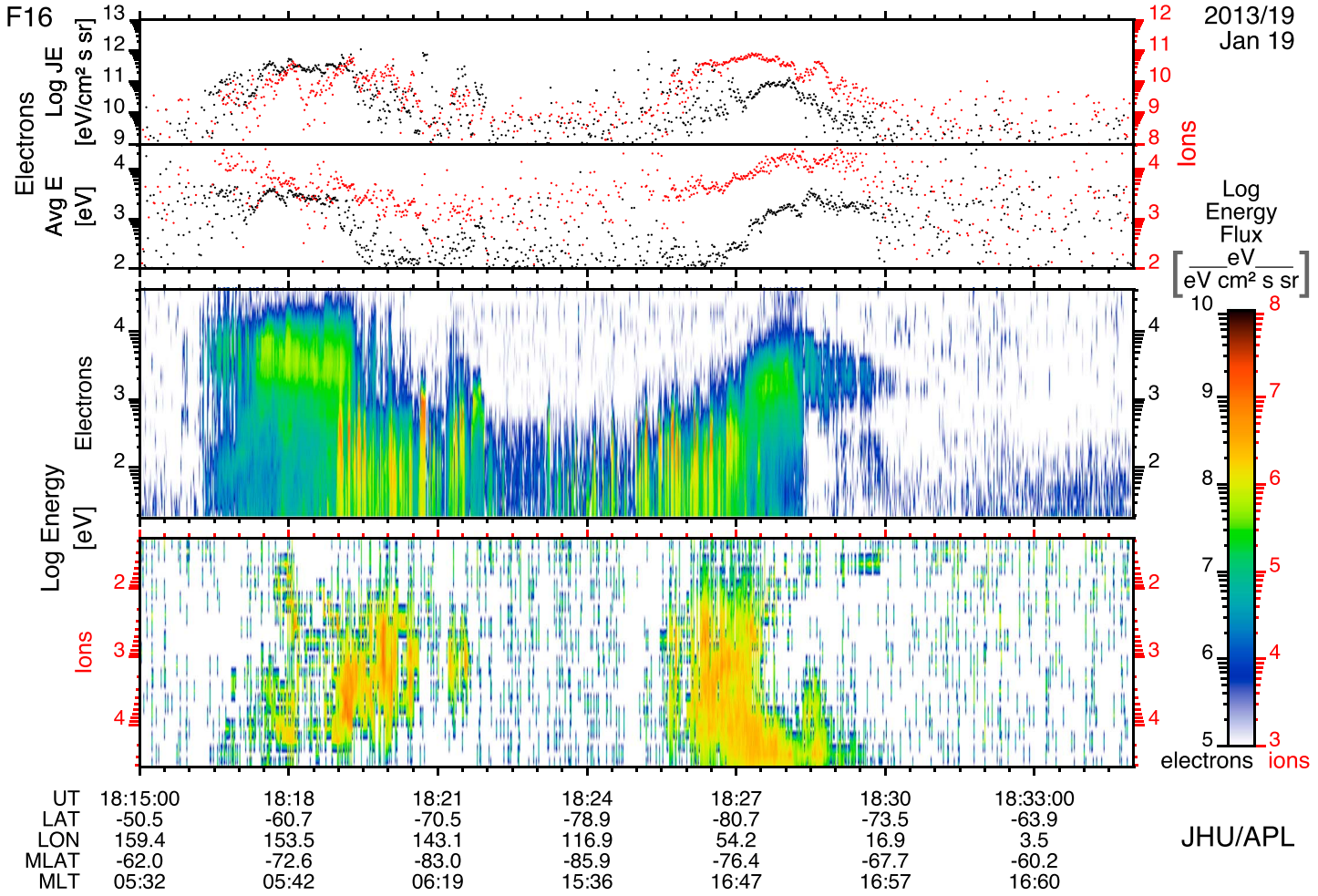

Figure 9. Spectrograms of electron and ion flux data from DMSP-F16. From top to bottom: (first panel) Particle flux intensities of electrons and ions, (second panel) average energy of the particles, and (third panel) spectrograms for electrons and ions.

solar wind conditions and geomagnetic activities [e.g., *Engebretson et al.*, 2008], prohibiting efficient propagation in the waveguide (see *Urban et al.* [2016] for discussions of the station's location in the open field lines). We emphasize, however, that the data show very efficient ionospheric waveguide propagation over a large latitudinal extent from −62° MLAT (HBA) to −80° MLAT (AGO1).

The companion paper by *Kim et al.* [2015] reported that the TCV centers during Event 1 and Event 2 were 73.5° MLAT and 72.0° MLAT, respectively, and the latitude of the transient compression events observed by THEMIS coincided approximately with that of the TCV center. These locations are similar to the estimated wave source locations based on the ground data. Figure 8 presents three-dimensional ion velocity distributions calculated from ion fluxes measured by the electrostatic analyzer (ESA) aboard the THEMIS D spacecraft. The measurement times for each panel are marked in Figure 3 with dashed vertical lines (i) to (v). The *x* and *y* axis of the plots represent parallel and perpendicular components of ion velocities, respectively. The flux levels are color coded. Lines (i) and (ii) show velocity distributions just before and after the transient compression for Event 1. Similarly, the velocity distributions shown in line (iii) were obtained before the transient compression and those in lines (iv) and (v) after the transient phenomena for Event 2. Although most of the distributions display slightly anisotropic distributions ($v_\perp > v_\parallel$), no remarkable changes are found between the times before and after the onset. This does not necessarily negate the possibility of wave generation triggered by the transient compression because the wave source locations may not coincide with the transient compression in *L* shell. Another scenario might be that the waves act quickly to limit the proton anisotropy toward conditions of marginal stability as suggested by *Gary et al.* [1994]. Again, we note that there are no other THEMIS data available to show wave events.

A simulation study by *Lysak and Lee* [1992] has shown that a pressure pulse at the magnetopause generates a compressional wave, which propagates across field lines through the magnetosphere, creating vortex structures in the ionosphere. They also showed that shear Alfvén waves are generated from the compressional waves due to magnetospheric inhomogeneity, consequently driving FACs. Thus, we suggest here that it is possible that EMIC wave source locations are inward from the transient phenomena near the magnetopause. For Event 2, in particular, the GOES 13 spacecraft also measured EMIC waves. Combining this with the ground observations, we conclude that the Event 2 waves, which are associated with higher P_d change, occurred over a large latitudinal extent ($L = \sim 6-10$).

We used DMSP F16 particle flux data to examine the source region because localized precipitation of energetic (>10 keV) protons is known to be correlated with EMIC waves [e.g., *Yahnin and Yahnina*, 2007; *Engebretson et al.*, 2013]. Figure 5 shows the magnetic footprint of the low Earth orbiting spacecraft during Event 2 (~18:20–18:30 UT). The spectrograms from the DMSP-F16 spacecraft in Figure 9 display a clear isolated burst of precipitating protons (>10 keV) approximately between 18:27 and 18:29 UT, which corresponds to the region between SPA and AGO3 (STF and IQA) latitudinally (see the DMSP F16 spacecraft magnetic footprint in Figure 5). The observation of electron precipitation supports the localization of the wave source from ground observations to be near the TCV center.

5. Conclusions

EMIC waves associated with transient changes in solar wind and TCV events are reported in this paper. A thorough investigation of the TCV events is reported by the companion paper by *Kim et al.* [2015]. The THEMIS spacecraft fortuitously located near the magnetopause observed radial fluctuations of the magnetopause in response to sudden increases in P_d, and the interhemispheric conjugate ground-based magnetometers measured well-defined EMIC waves during quiet times. The sequence of events described in this paper and conclusions are as follows:

1. Solar wind data (OMNI) show two consecutive transient increases in P_d.
2. Radial fluctuations of the magnetopause corresponding to the P_d increases were observed by the three THEMIS spacecraft near the magnetopause.
3. Both the *SYM-H* index and GOES magnetometer data presented sudden compression of the magnetosphere in association with the transient events.
4. EMIC waves were observed by the interhemispheric ground magnetometer network as well as the GOES spacecraft in association with the transient phenomena, suggesting that waves occurred over an extensive latitudinal ($L = \sim 6-10$) and longitudinal (~6 h in MLT) range.
5. The wave features were remarkably similar in conjugate hemispheres in terms of bandwidth, quasiperiodic wave power modulation, and polarization.
6. The spectral structures of the waves appeared to be well correlated with the fluctuating motion of the magnetopause: the waves were modulated with the quasiperiodic boundary motion, showing compression-associated wave generation.
7. Using data from the latitudinally extensive magnetometer network and the particle flux instrument aboard the DMSP spacecraft, the wave source region was estimated to be near the TCV center (72° – 74° MLT).
8. The confluence of space-borne and ground instruments including the interhemispheric, high-latitude, fluxgate/induction coil magnetometer array allows us to constrain the EMIC source region while also confirming the relationship between EMIC waves and the TCV current system.
9. The solar wind buffeting in association with transient P_d increases, albeit not very strong during quiet times, provides energy to generate or enhance EMIC waves over a large radial and local time extent.

Acknowledgments
The work at New Jersey Institute of Technology was supported by National Science Foundation (NSF) grant AGS-1547252. The work at Virginia Tech was supported by NSF grant PLR-1543364. The fluxgate magnetometer projects at SPA and AGOs are supported by NSF grants PLR-1247975 and PLR-1443507, respectively, to New Jersey Institute of Technology. The induction coil magnetometer projects at STF, IQA, SPA, and AGOs are supported by NSF grants PLR-1341677 to the University of New Hampshire and PLR-1341493 to Augsburg College. The authors would like to thank the following persons/institutes for providing data: the THEMIS team for fluxgate magnetometer and electrostatic analyzer data; the NOAA GOES team for fluxgate magnetometer data; the DMSP team for SSJ particle data; Lorne McKee at Natural Resources Canada (NRCan) and INTERMAGNET for fluxgate magnetometer data from IQA, which is operated by NRCan; the Technical University of Denmark National Space Institute (DTU Space) for the fluxgate magnetometer data (STF); the British Antarctic Survey (BAS) team for fluxgate data (HBA); and the AGO project team for operations of the magnetometer stations. All data used in this study can be obtained from the following data repositories and tools: OMNI, ACE, and THEMIS data from the NASA Coordinated Data Analysis Web (CDAWeb) at http://cdaweb.sci.gsfc.nasa.gov and Space Physics Environment Data Analysis Software (SPEDAS); GOES magnetometer data from the data archive at National Oceanic and Atmospheric Administration (NOAA) National Centers for Environmental Information (NCEI, previously known as NGDC) (http://satdat.ngdc.noaa.gov/sem/goes/data/new_full/); DMSP particle data from the DMSP Online Spectrogram Viewer Tool at http://sd-www.jhuapl.edu/Aurora/spectrogram/index.html; IQA fluxgate data from the Intermagnet (www.intermagnet.org); STF fluxgate magnetometer data from the DTU database (https://ftp.space.dtu.dk/data/Ground_magnetometers/Adjusted/); HBA fluxgate data from the BAS Data Access System (http://psddb.nerc-bas.ac.uk); and SPA and AGO fluxgate and induction coil magnetometer data from the New Jersey Institute of Technology database (www.antarcticgeospace.org).

References

Amm, O., M. J. Engebretson, T. Hughes, L. Newitt, A. Viljanen, and J. Watermann (2002), A traveling convection vortex event study: Instantaneous ionospheric equivalent currents, estimation of field-aligned currents, and the role of induced currents, *J. Geophys. Res.*, *107*, 1334, doi:10.1029/2002JA009472.

Anderson, B. J., and D. C. Hamilton (1993), Electromagnetic ion cyclotron waves stimulated by modest magnetospheric compressions, *J. Geophys. Res.*, *98*, 11,369–11,382, doi:10.1029/93JA00605.

Anderson, B. J., R. E. Erlandson, and L. J. Zanetti (1992), A statistical study of Pc 1–2 magnetic pulsations in the equatorial magnetosphere. 1. Equatorial occurrence distributions., *J. Geophys. Res.*, *97*, 3075–3088, doi:10.1029/91JA02706.

Anderson, B. J., R. E. Denton, G. Ho, D. C. Hamilton, S. A. Fuselier, and R. J. Strangeway (1996), Observational test of local proton cyclotron instability in the Earth's magnetosphere, *J. Geophys. Res.*, *101*, 21,527–21,544, doi:10.1029/96JA01251.

Angelopoulos, V. (2008), The THEMIS mission, *Space Sci. Rev.*, *141*, 5–34, doi:10.1007/s11214-008-9336-1.

Arnoldy, R. L., M. J. Engebretson, and L. J. Cahill Jr. (1988), Bursts of Pc 1–2 near the ionospheric footprint of the cusp and their relationship to flux transfer events, *J. Geophys. Res.*, *93*, 1007–1016, doi:10.1029/JA093iA02p01007.

Arnoldy, R. L., M. J. Engebretson, J. L. Alford, R. E. Erlandson, and B. J. Anderson (1996), Magnetic impulse events and associated Pc 1 bursts at dayside high latitudes, *J. Geophys. Res.*, *101*, 7793–7800, doi:10.1029/95JA03378.

Auster, H. U., et al. (2008), The THEMIS fluxgate magnetometer, *Space Sci. Rev.*, *141*, 235–264, doi:10.1007/s11214-008-9365-9.

Cho, J.-H., D.-Y. Lee, S.-J. Noh, D.-K. Shin, J. Hwang, K.-C. Kim, J. J. Lee, C. R. Choi, S. Thaller, and R. Skoug (2016), Van Allen Probes observations of electromagnetic ion cyclotron waves triggered by enhanced solar wind dynamic pressure, *J. Geophys. Res. Space Physics*, *121*, 9771–9793, doi:10.1002/2016JA022841.

Claudepierre, S. G., S. R. Elkington, and M. Wiltberger (2008), Solar wind driving of magnetospheric ULF waves: Pulsations driven by velocity shear at the magnetopause, *J. Geophys. Res.*, *113*, A05218, doi:10.1029/2007JA012890.

Clauer, C. R. (2003), Ionospheric observations of waves at the inner edge of the low latitude boundary layer, in *Earth's Low-Latitude Boundary Layer, Geophys. Monogr. Ser.*, vol. 133, pp. 297–309, AGU, Washington, D. C., doi:10.1029/133GM30.

Clauer, C. R., and A. J. Ridley (1995), Ionospheric observations of magnetospheric low-latitude boundary layer waves on August 4, 1991, *J. Geophys. Res.*, *100*, 21,873–21,884, doi:10.1029/95JA00678.

Clauer, C. R., H. Kim, K. Deshpande, Z. Xu, D. Weimer, S. Musko, G. Crowley, C. Fish, R. Nealy, T. E. Humphreys, J. A. Bhatti, and A. J. Ridley (2014), An autonomous adaptive low-power instrument platform (AAL-PIP) for remote high-latitude geospace data collection, *Geosci. Instrum. Method. Data Syst.*, *3*, 211–227, doi:10.5194/gi-3-211-2014.

Clausen, L. B. N., J. B. H. Baker, J. M. Ruohoniemi, and H. J. Singer (2011), EMIC waves observed at geosynchronous orbit during solar minimum: Statistics and excitation, *J. Geophys. Res.*, *116*, A10205, doi:10.1029/2011JA016823.

Engebretson, M. J., W. K. Peterson, J. L. Posch, M. R. Klatt, B. J. Anderson, C. T. Russell, H. J. Singer, R. L. Arnoldy, and H. Fukunishi (2002), Observations of two types of Pc 1–2 pulsations in the outer dayside magnetosphere, *J. Geophys. Res.*, *107*, 1451, doi:10.1029/2001JA000198.

Engebretson, M. J., M. R. Lessard, J. Bortnik, J. C. Green, R. B. Horne, D. L. Detrick, A. T. Weatherwax, J. Manninen, N. J. Petit, J. L. Posch, and M. C. Rose (2008), Pc1–Pc2 waves and energetic particle precipitation during and after magnetic storms: Superposed epoch analysis and case studies, *J. Geophys. Res.*, *113*, A01211, doi:10.1029/2007JA012362.

Engebretson, M. J., et al. (2013), Multi-instrument observations from Svalbard of a traveling convection vortex, electromagnetic ion cyclotron wave burst, and proton precipitation associated with a bow shock instability, *J. Geophys. Res. Space Physics*, *118*, 2975–2997, doi:10.1002/jgra.50291.

Fairfield, D. H. (1971), Average and unusual locations of the Earth's magnetopause and bow shock, *J. Geophys. Res.*, *76*, 6700–6716, doi:10.1029/JA076i028p06700.

Fillingim, M. O., J. P. Eastwood, G. K. Parks, V. Angelopoulos, I. R. Mann, S. B. Mende, and A. T. Weatherwax (2011), Polar UVI and THEMIS GMAG observations of the ionospheric response to a hot flow anomaly, *J. Atmos. Sol. Terr. Phys.*, *73*, 137–145, doi:10.1016/j.jastp.2010.03.001.

Fraser, B. J. (1975), Ionospheric duct propagation and Pc 1 pulsation sources, *J. Geophys. Res.*, *80*, 2790–2796, doi:10.1029/JA080i019p02790.

Friis-Christensen, E., S. Vennerstrom, M. A. McHenry, and C. R. Clauer (1988), Ionospheric traveling convection vortices observed near the polar cleft—A triggered response to sudden changes in the solar wind, *Geophys. Res. Lett.*, *15*, 253–256, doi:10.1029/GL015i003p00253.

Fujita, S., and T. Tamao (1988), Duct propagation of hydromagnetic waves in the upper ionosphere. I—Electromagnetic field disturbances in high latitudes associated with localized incidence of a shear Alfvén wave, *J. Geophys. Res.*, *93*, 14,665–14,673, doi:10.1029/JA093iA12p14665.

Fujita, S., K. H. Glassmeier, and K. Kamide (1996), MHD waves generated by the Kelvin-Helmholtz instability in a nonuniform magnetosphere, *J. Geophys. Res.*, *101*, 27,317–27,326, doi:10.1029/96JA02676.

Gary, S. P., M. B. Moldwin, M. F. Thomsen, D. Winske, and D. J. McComas (1994), Hot proton anisotropies and cool proton temperatures in the outer magnetosphere, *J. Geophys. Res.*, *99*, 23,603–23,615, doi:10.1029/94JA02069.

Glassmeier, K.-H., and C. Heppner (1992), Traveling magnetospheric convection twin vortices—Another case study, global characteristics, and a model, *J. Geophys. Res.*, *97*, 3977–3992, doi:10.1029/91JA02464.

Glassmeier, K.-H., M. Hoenisch, and J. Untiedt (1989), Ground-based and satellite observations of traveling magnetospheric convection twin vortices, *J. Geophys. Res.*, *94*, 2520–2528, doi:10.1029/JA094iA03p02520.

Halford, A. J., B. J. Fraser, and S. K. Morley (2010), EMIC wave activity during geomagnetic storm and nonstorm periods: CRRES results, *J. Geophys. Res.*, *115*, A12248, doi:10.1029/2010JA015716.

Halford, A. J., B. J. Fraser, and S. K. Morley (2015), EMIC waves and plasmaspheric and plume density: CRRES results, *J. Geophys. Res. Space Physics*, *120*, 1974–1992, doi:10.1002/2014JA020338.

Hartinger, M. D., V. Angelopoulos, M. B. Moldwin, K. Takahashi, and L. B. N. Clausen (2013), Statistical study of global modes outside the plasmasphere, *J. Geophys. Res. Space Physics*, *118*, 804–822, doi:10.1002/jgra.50140.

Hartinger, M. D., F. Plaschke, M. O. Archer, D. T. Welling, M. B. Moldwin, and A. Ridley (2015), The global structure and time evolution of dayside magnetopause surface eigenmodes, *Geophys. Res. Lett.*, *42*, 2594–2602, doi:10.1002/2015GL063623.

Hasegawa, H., M. Fujimoto, T.-D. Phan, H. Rème, A. Balogh, M. W. Dunlop, C. Hashimoto, and R. TanDokoro (2004), Transport of solar wind into Earth's magnetosphere through rolled-up Kelvin-Helmholtz vortices, *Nature*, *430*, 755–758, doi:10.1038/nature02799.

Jordanova, V. K., C. J. Farrugia, R. M. Thorne, G. V. Khazanov, G. D. Reeves, and M. F. Thomsen (2001), Modeling ring current proton precipitation by electromagnetic ion cyclotron waves during the May 14–16, 1997, storm, *J. Geophys. Res.*, *106*, 7–22, doi:10.1029/2000JA002008.

Jordanova, V. K., D. T. Welling, S. G. Zaharia, L. Chen, and R. M. Thorne (2012), Modeling ring current ion and electron dynamics and plasma instabilities during a high-speed stream driven storm, *J. Geophys. Res.*, *117*, A00L08, doi:10.1029/2011JA017433.

Kataoka, R., H. Fukunishi, L. J. Lanzerotti, C. G. Maclennan, H. U. Frey, S. B. Mende, J. H. Doolittle, T. J. Rosenberg, and A. T. Weatherwax (2001), Magnetic impulse event: A detailed case study of extended ground and space observations, *J. Geophys. Res.*, *106*, 25,873–25,890, doi:10.1029/2000JA000314.

Kim, H., M. R. Lessard, M. J. Engebretson, and H. Lühr (2010), Ducting characteristics of Pc 1 waves at high latitudes on the ground and in space, *J. Geophys. Res.*, *115*, A09310, doi:10.1029/2010JA015323.

Kim, H., M. R. Lessard, M. J. Engebretson, and M. A. Young (2011), Statistical study of Pc1–2 wave propagation characteristics in the high-latitude ionospheric waveguide, *J. Geophys. Res.*, *116*, A07227, doi:10.1029/2010JA016355.

Kim, H., X. Cai, C. R. Clauer, B. S. R. Kunduri, J. Matzka, C. Stolle, and D. R. Weimer (2013), Geomagnetic response to solar wind dynamic pressure impulse events at high-latitude conjugate points, *J. Geophys. Res. Space Physics*, *118*, 6055–6071, doi:10.1002/jgra.50555.

Kim, H., C. R. Clauer, M. J. Engebretson, J. Matzka, D. G. Sibeck, H. J. Singer, C. Stolle, D. R. Weimer, and Z. Xu (2015), Conjugate observations of traveling convection vortices associated with transient events at the magnetopause, *J. Geophys. Res. Space Physics*, *120*, 2015–2035, doi:10.1002/2014JA020743.

Kim, K.-H., J.-S. Park, Y. Omura, K. Shiokawa, D.-H. Lee, G.-J. Kim, H. Jin, E. Lee, and H.-J. Kwon (2016), Spectral characteristics of steady quiet-time EMIC waves observed at geosynchronous orbit, *J. Geophys. Res.*, *121*, 8640–8660, doi:10.1002/2016JA022957.

King, J. H., and N. E. Papitashvili (2005), Solar wind spatial scales in and comparisons of hourly Wind and ACE plasma and magnetic field data, *J. Geophys. Res.*, *110*, A02104, doi:10.1029/2004JA010649.

Kivelson, M. G., and D. J. Southwood (1991), Ionospheric traveling vortex generation by solar wind buffeting of the magnetosphere, *J. Geophys. Res.*, *96*, 1661–1667, doi:10.1029/90JA01805.

Kozyra, J. U., V. K. Jordanova, R. B. Horne, and R. M. Thorne (1997), Modeling of the contribution of electromagnetic ion cyclotron (EMIC) waves to stormtime ring current erosion, in *Magnetic Storms, Geophys. Monogr. Ser.*, vol. 98, edited by B. T. Tsurutani et al., pp. 187–202, AGU, Washington, D. C.

Loto'Aniu, T. M., B. J. Fraser, and C. L. Waters (2009), The modulation of electromagnetic ion cyclotron waves by Pc 5 ULF waves, *Ann. Geophys.*, *27*, 121–130, doi:10.5194/angeo-27-121-2009.

Lyons, L. R., and R. M. Thorne (1972), Parasitic pitch angle diffusion of radiation belt particles by ion cyclotron waves, *J. Geophys. Res.*, *77*, 5608–5616, doi:10.1029/JA077i028p05608.

Lysak, R. L., and D.-H. Lee (1992), Response of the dipole magnetosphere to pressure pulses, *Geophys. Res. Lett.*, *19*, 937–940, doi:10.1029/92GL00625.

McFadden, J. P., C. W. Carlson, D. Larson, J. Bonnell, F. Mozer, V. Angelopoulos, K.-H. Glassmeier, and U. Auster (2008), THEMIS ESA first science results and performance issues, *Space Sci. Rev.*, *141*, 477–508, doi:10.1007/s11214-008-9433-1.

McHenry, M. A., and C. R. Clauer (1987), Modeled ground magnetic signatures of flux transfer events, *J. Geophys. Res.*, *92*, 11,231–11,240, doi:10.1029/JA092iA10p11231.

McHenry, M. A., C. R. Clauer, E. Friis-Christensen, P. T. Newell, and J. D. Kelly (1990), Ground observations of magnetospheric boundary layer phenomena, *J. Geophys. Res.*, *95*, 14,995–15,005, doi:10.1029/JA095iA09p14995.

Melville, R., A. Stillinger, A. Gerrard, and A. Weatherwax (2014), Sustainable energy at the 100 W level for scientific sites on the Antarctic Plateau: Lessons learned from the Polar Experiment Network for Geospace Upper Atmosphere Investigations-Automatic Geophysical Observatory project, *Rev. Sci. Instrum.*, *85*(4), 45117, doi:10.1063/1.4871555.

Mende, S. B., et al. (2009), Observations of Earth space by self-powered stations in Antarctica, *Rev. Sci. Instrum.*, *80*(12), 124,501–124,501, doi:10.1063/1.3262506.

Murr, D. L., W. J. Hughes, A. S. Rodger, E. Zesta, H. U. Frey, and A. T. Weatherwax (2002), Conjugate observations of traveling convection vortices: The field-aligned current system, *J. Geophys. Res.*, *107*, 1306, doi:10.1029/2002JA009456.

Musko, S. B., C. R. Clauer, A. J. Ridley, and K. L. Arnett (2009), Autonomous low-power magnetic data collection platform to enable remote high latitude array deployment, *Rev. Sci. Instrum.*, *80*, 44501, doi:10.1063/1.3108527.

Park, J.-S., K.-H. Kim, K. Shiokawa, D.-H. Lee, E. Lee, H.-J. Kwon, H. Jin, and G. Jee (2016), EMIC waves observed at geosynchronous orbit under quiet geomagnetic conditions ($Kp \leq 1$), *J. Geophys. Res. Space Physics*, *121*, 1377–1390, doi:10.1002/2015JA021968.

Piersanti, M., U. Villante, C. Waters, and I. Coco (2012), The 8 June 2000 ULF wave activity: A case study, *J. Geophys. Res.*, *117*, A02204, doi:10.1029/2011JA016857.

Posch, J. L., M. J. Engebretson, A. J. Witte, D. L. Murr, M. R. Lessard, M. G. Johnsen, H. J. Singer, and M. D. Hartinger (2013), Simultaneous traveling convection vortex events and Pc1 wave bursts at cusp latitudes observed in Arctic Canada and Svalbard, *J. Geophys. Res. Space Physics*, *118*, 6352–6363, doi:10.1002/jgra.50604.

Rasinkangas, R., and K. Mursula (1998), Modulation of magnetospheric EMIC waves by Pc 3 pulsations of upstream origin, *Geophys. Res. Lett.*, *25*, 869–872, doi:10.1029/98GL50415.

Saikin, A. A., J.-C. Zhang, C. W. Smith, H. E. Spence, R. B. Torbert, and C. A. Kletzing (2016), The dependence on geomagnetic conditions and solar wind dynamic pressure of the spatial distributions of EMIC waves observed by the Van Allen Probes, *J. Geophys. Res. Space Physics*, *121*, 4362–4377, doi:10.1002/2016JA022523.

Shi, Q. Q., et al. (2013), THEMIS observations of ULF wave excitation in the nightside plasma sheet during sudden impulse events, *J. Geophys. Res. Space Physics*, *118*, 284–298, doi:10.1029/2012JA017984.

Shprits, Y. Y., et al. (2016), Wave-induced loss of ultra-relativistic electrons in the Van Allen radiation belts, *Nat. Commun.*, *7*, 12883, doi:10.1038/ncomms12883.

Shue, J.-H., J. K. Chao, H. C. Fu, C. T. Russell, P. Song, K. K. Khurana, and H. J. Singer (1997), A new functional form to study the solar wind control of the magnetopause size and shape, *J. Geophys. Res.*, *102*, 9497–9512, doi:10.1029/97JA00196.

Sibeck, D. G., R. E. Lopez, and W. Baumjohann (1989), Solar wind dynamic pressure variations and transient magnetospheric signatures, *Geophys. Res. Lett.*, *16*, 13–16, doi:10.1029/GL016i001p00013.

Sibeck, D. G., N. B. Trivedi, E. Zesta, R. B. Decker, H. J. Singer, A. Szabo, H. Tachihara, and J. Watermann (2003), Pressure-pulse interaction with the magnetosphere and ionosphere, *J. Geophys. Res.*, *108*, 1095, doi:10.1029/2002JA009675.

Sitar, R. J., J. B. Baker, C. R. Clauer, A. J. Ridley, J. A. Cumnock, V. O. Papitashvili, J. Spann, M. J. Brittnacher, and G. K. Parks (1998), Multi-instrument analysis of the ionospheric signatures of a hot flow anomaly occurring on July 24, 1996, *J. Geophys. Res.*, *103*, 23,357–23,372, doi:10.1029/98JA01916.

Summers, D., and R. M. Thorne (2003), Relativistic electron pitch-angle scattering by electromagnetic ion cyclotron waves during geomagnetic storms, *J. Geophys. Res.*, *108*, 1143, doi:10.1029/2002JA009489.

Summers, D., B. Ni, and N. P. Meredith (2007a), Timescales for radiation belt electron acceleration and loss due to resonant wave-particle interactions: 1. Theory, *J. Geophys. Res.*, *112*, A04206, doi:10.1029/2006JA011801.

Summers, D., B. Ni, and N. P. Meredith (2007b), Timescales for radiation belt electron acceleration and loss due to resonant wave-particle interactions: 2. Evaluation for VLF chorus, ELF hiss, and electromagnetic ion cyclotron waves, *J. Geophys. Res.*, *112*, A04207, doi:10.1029/2006JA011993.

Thorne, R. M., and C. F. Kennel (1971), Relativistic electron precipitation during magnetic storm main phase, *J. Geophys. Res.*, *76*, 4446–4453, doi:10.1029/JA076i019p04446.

Thorne, R. M., R. B. Horne, V. K. Jordanova, J. Bortnik, and S. Glauert (2006), Interaction of EMIC waves with thermal plasma and radiation belt particles, in *Magnetospheric ULF Waves: Synthesis and New Directions, Geophys. Monogr. Ser.*, vol. 169, edited by K. Takahashi, pp. 213–223, AGU, Washington, D. C.

Tsyganenko, N. A. (2002a), A model of the near magnetosphere with a dawn-dusk asymmetry 1. Mathematical structure, *J. Geophys. Res.*, *107*, 1179, doi:10.1029/2001JA000219.

Tsyganenko, N. A. (2002b), A model of the near magnetosphere with a dawn-dusk asymmetry 2. Parameterization and fitting to observations, *J. Geophys. Res.*, *107*, 1176, doi:10.1029/2001JA000220.

Urban, K. D., A. J. Gerrard, L. J. Lanzerotti, and A. T. Weatherwax (2016), Rethinking the polar cap: Eccentric dipole structuring of ULF power at the highest corrected geomagnetic latitudes, *J. Geophys. Res. Space Physics*, *121*, 8475–8507, doi:10.1002/2016JA022567.

Usanova, M. E., I. R. Mann, I. J. Rae, Z. C. Kale, V. Angelopoulos, J. W. Bonnell, K.-H. Glassmeier, H. U. Auster, and H. J. Singer (2008), Multipoint observations of magnetospheric compression-related EMIC Pc1 waves by THEMIS and CARISMA, *Geophys. Res. Lett.*, *35*, L17S25, doi:10.1029/2008GL034458.

Usanova, M. E., et al. (2010), Conjugate ground and multisatellite observations of compression-related EMIC Pc1 waves and associated proton precipitation, *J. Geophys. Res.*, *115*, A07208, doi:10.1029/2009JA014935.

Usanova, M. E., I. R. Mann, J. Bortnik, L. Shao, and V. Angelopoulos (2012), THEMIS observations of electromagnetic ion cyclotron wave occurrence: Dependence on AE, SYMH, and solar wind dynamic pressure, *J. Geophys. Res.*, *117*, A10218, doi:10.1029/2012JA018049.

Yahnin, A., and T. Yahnina (2007), Energetic proton precipitation related to ion cyclotron waves, *J. Atmos. Sol. Terr. Phys.*, *69*, 1690–1706, doi:10.1016/j.jastp.2007.02.010.

Zesta, E., W. J. Hughes, M. J. Engebretson, T. J. Hughes, A. J. Lazarus, and K. I. Paularena (1999), The November 9, 1993, traveling convection vortex event: A case study, *J. Geophys. Res.*, *104*, 28,041–28,058, doi:10.1029/1999JA900306.

Zesta, E., W. J. Hughes, and M. J. Engebretson (2002), A statistical study of traveling convection vortices using the Magnetometer Array for Cusp and Cleft Studies, *J. Geophys. Res.*, *107*, 1317, doi:10.1029/1999JA000386.